Magnetic moment and coupling mechanism of iron-doped rutile TiO_2 from first principles

G. Mallia[1,*] and N. M. Harrison[1,2]
[1]*Department of Chemistry, Imperial College London, South Kensington London SW7 2AZ, United Kingdom*
[2]*Daresbury Laboratory, Daresbury, Warrington, WA4 4AD, United Kingdom*
(Received 14 December 2006; revised manuscript received 7 February 2007; published 2 April 2007)

The magnetic ground state of Fe-doped rutile TiO_2, an oxide-based dilute magnetic semiconductor, has been investigated within the hybrid-exchange approximation to density-functional theory. $Fe_xTi_{1-x}O_2$ with $x=0.125$ has been simulated by means of a 24-atom supercell with Fe doped substitutionally for Ti and this is established as the dilute limit through explicit comparison with calculations on a 192-atom supercell ($x=0.0156$). A detailed study of the nature and stability of the predicted ground state with respect to variations in the oxidation state of the Fe ion, the delocalization or self-trapping of holes donated to the lattice, and the treatment of electronic exchange and correlation is presented. The ground state is found to be well described by a model based on an Fe^{3+}-d^5 in a high spin state coupled to a partially delocalized hole accommodated in the $2p$ states of neighboring oxygen ions. No evidence is found for ferromagnetic coupling suggesting that the observed ferromagnetism in this system is dependent upon additional structural and/or electronic defects.

DOI: 10.1103/PhysRevB.75.165201 PACS number(s): 75.30.Hx, 71.20.Nr, 71.15.Mb

I. INTRODUCTION

Titanium dioxide has a variety of interesting physical and chemical properties and has therefore been extensively studied experimentally (see review and references in Ref. 1) and using a range of theoretical approaches (i.e., Refs. 2–12). Recently, it has been observed that when doping TiO_2 with transition metal (TM) impurities at low concentration ($Ti_{1-x}X_xO_2$, with X=TM and x from 0.01 up to 0.14), titanium dioxide exhibits room temperature (RT) ferromagnetism.[13–32] In addition, for iron ($x\sim0.07$)[31,33] and cobalt ($x\leq0.12$)[13–15] doping of thin films the material remains transparent. The doped material has potential for use in spintronics and optoelectronics if the ferromagnetism can be understood and controlled.[34]

The origin of the RT ferromagnetism has been studied using a number of experimental techniques but there is still no clear consensus about the resultant lattice structure, the sites adopted by TM ions, the distribution of the ions in the lattice, their oxidation state, or the magnetic moment per ion. Transition electron microscopy (TEM),[13,14,17,18,26,27] scanning electron microscopy (SEM),[14,23,24] and atomic force microscopy (AFM)[14] have been used to demonstrate the solubility of TM atoms in various forms of TiO_2 at a variety of concentrations, for which no sign of segregation of an impurity phase is evident. This conclusion has been corroborated by x-ray diffraction (XRD) data, which is consistent with the incorporation of TM ions into both anatase and rutile lattices.[13–15,17,18,25–27,32]

In the case of Fe, XRD,[22–24,28,35–37] Raman,[31,38] and Mössbauer spectra[25,37,39,40] indicate that Fe is incorporated substitutionally for Ti. Analysis of the Mössbauerlast data suggests the presence of both Fe^{2+} and Fe^{3+} species[25,37,39,40] while x-ray photoemission spectroscopy (XPS) indicates that Fe is in the 3+ state only.[32] Electron paramagnetic resonance (EPR) implies that in rutile Fe^{3+} substitutes for Ti^{4+}.[41,42] It is the doping of rutile that is of the most immediate interest as it is the thermodynamically most stable phase and thus the most promising for applications of titania as a high-T_C dilute magnetic semiconductor.[24]

The magnetic moment of the Fe species appears to be very sensitive to the details of the preparation and form of rutile and a very wide range of magnetic moments ($0.05-2.5\mu_B$) have been reported. In rutile powder with Fe at $x=0.01$, the magnetic hysteresis at RT displays ferromagnetic behavior with a magnetic moment of about $0.68\mu_B$/Fe.[25] In rutile thin films at $x=0.06$, a magnetic moment of $1.3\mu_B$/Fe[32] has been deduced from superconducting quantum interference device (SQUID) measurements. In rutile films with similar Fe content ($x=0.081$) the observed moment is significally smaller ($\sim0.15\mu_B$/Fe), and has been observed to decrease to $0.051\mu_B$/Fe at higher concentrations ($x=0.126$).[24,28] In vacuum-annealed rutile films with $x=0.05$, the SQUID measurements imply a moment of $0.48\mu_B$/Fe.[31] In reduced-rutile thin films with $x=0.02$, 0.06, and 0.08, at 300 K exhibit hysteresis with a saturation magnetization of $2.3-2.4\mu_B$ per Fe atom.[17,18]

In all of the studies discussed above the Fe dopants were considered to be incorporated in the rutile lattice but there have been a number of reports which challenge this interpretation. (1) In rutile films with $x=\sim0.07$ the magnetic behavior has been attributed to the presence of Fe_3O_4 nanoparticles revealed by AFM, SEM, TEM, XPS, and x-ray absorption near-edge spectroscopy measurements.[43] (2) In Fe-doped TiO_2 nanopowders with particle sizes of 10–100 nm and x ranging from 0 to 0.20, a purely paramagnetic response was observed at RT.[37,40]

A number of theoretical studies have been performed in order to characterize these materials. The full-potential linearized-augmented plane wave method, both in the local density (LDA) and generalized gradient (GGA) approximations, has been used to study the magnetic order in $Fe_{0.5}Ti_{0.5}O_2$. At this high concentration three different magnetic orderings were studied in supercells containing four formula units and the ground state was found to be antiferromagnetic although a metastable phase with weak ferromagnetic coupling along the crystallographic **a** direction was also seen.[44,45] Interestingly the computed magnetic moment was sensitive to the distribution of iron in the supercells

varying in the range $1.68-2.67\mu_B$/Fe. However, these calculations assumed a high-spin oxidation state of Fe^{4+} (with a formal value $|S_{Fe}|=2$) in the analysis of the magnetic coupling and were restricted to concentrations much higher than those observed. In a related study the electronic structure was studied at lower concentrations ($x=0.25$ and 0.0625) and, for similar local geometries the magnetic moment per Fe was found to be insensitive to the concentration.[45,46] The high concentration phase $Fe_{0.5}Ti_{0.5}O_2$ (equivalent to $FeTiO_4$, of course) can be compared with ilmenite ($FeTiO_3$), a mineral that can be thought of as a stable, oxygen deficient phase, occurring at very high x.

In the current content ilmenite is an interesting reference as within the ionic model there are two distinct cation charge orderings consistent with O^{2-}, i.e., $Fe^{2+}Ti^{4+}$ and $Fe^{3+}Ti^{3+}$ and the charge transfer excitation between the antiferromagnetic Fe^{2+}-d^6 ground state and the Fe^{3+}-d^5 state has been observed and reproduced in hybrid exchange DFT calculations.[47]

This method is also adopted in the current work as it has been proven to provide a reliable approach to the electronic structure, orbital and magnetic ordering in a wide variety of transition metal oxides overcoming the well-established problems suffered by LDA and GGA approaches which underestimate band gaps and overestimate magnetic couplings.[47–55] In these materials this is crucial as a correct description of the balance between localized and delocalized states is vital if the formation of hole states within the oxygen p band to compensate for the presence of Fe^{2+} or Fe^{3+} dopant ions is to be computed reliably.

The paper is organized as follows. Section II contains computational details. In Sec. III A the perfect rutile structure is presented with the supercell adopted for the doped system. The oxidation state of the iron atom and the consequent presence of hole(s) in the system have been investigated in Sec. III B. In Sec. III C the optimized geometry for the lowest-energy oxidation state has been studied and a comparison between 24- and 192-atom supercell is given. The total and projected density of states are shown in Sec. III D and the interplay between electronic structure and geometry is analyzed. The possible solutions with a localized hole are described in Sec. III E. The ferromagnetic and antiferromagnetic phases are reported in Sec. III F with the aim of evaluating the exchange coupling constants J. The main conclusions of this study are summarized in Sec. IV.

II. COMPUTATIONAL DETAILS

All calculations have been performed using the CRYSTAL03 software package,[56] based on the expansion of the crystalline orbitals as a linear combination of a local basis set (BS) consisting of atom centered Gaussian orbitals. The titanium and oxygen atoms are described by a triple valence all-electron BS: an 86-411G** contraction (one s, four sp, and two d shells) and an 8-411G* contraction (one s, three sp, and one d shells), respectively;[57] the most diffuse sp (d) exponents are $\alpha^{Ti}=0.3297$ (0.26) and $\alpha^{O}=0.1843$(0.6) Bohr^{-2}. These basis sets were developed in previous studies of the bulk and surfaces phases of titania in which a systematic hierarchy of all-electron basis sets was used to quantify the effects of using a finite BS.[12,58] For the iron atom, in order to quantify the effects of the BS approximation on the delicate description of the different Fe oxidation states, two types of triple valence all-electron BS have been exploited:[59] one previously optimized in Fe^{3+} systems where the optimal most diffuse sp (d) exponents are $\alpha^{Ti}=0.5625$ (0.4345) Bohr^{-2} and one optimized for Fe^{2+} cases with the most diffuse sp (d) exponents being $\alpha^{Ti}=0.5306$ (0.321) Bohr^{-2}. The small changes in the exponents of the Fe^{3+}/Fe^{2+} basis sets indicate that the triple valence BS is adequately flexible to describe both oxidation states of Fe. For the 24-atom supercell considered below, the Fe^{3+} BS yields a total energy per cell some 0.24 eV ($9mE_h$)[85] lower than the Fe^{2+} BS and so the Fe^{3+} BS is used in all cases, with the Fe^{2+} BS used to check the sensitivity of key results only.

Electron exchange and correlation are approximated using the B3LYP hybrid exchange functional[60] which, as noted above, is expected to be more reliable than LDA or GGA approaches. The exchange-correlation potential and energy are integrated numerically on an atom centered grid of points. The integration over radial and angular coordinates is performed using Gauss-Legendre and Lebedev schemes, respectively. A pruned grid consisting of 75 radial points and 5 subintervals with (50,146,194,434,194) angular points has been used for all calculations (the LGRID option implemented in CRYSTAL03[56]). This grid converges the integrated charge density to 8×10^{-5} electrons per unit cell. The Coulomb and exchange series are summed directly and truncated using overlap criteria with thresholds of 10^{-7}, 10^{-7}, 10^{-7}, 10^{-7}, and 10^{-14} as described previously.[56,61] Reciprocal space sampling was performed on a Pack-Monkhorst net with a shrinking factor IS=8, which defines 75 symmetry unique k points in the bulk structure. The self-consistent field procedure was converged to a tolerance in the total energy of $\Delta E=1\times10^{-7}E_h$ per unit cell.

The TiO_2 cell parameters were optimized using numerical energy gradients with respect to the cell vectors. The internal coordinates for both the perfect and the Fe-doped system have been determined by minimization of the total energy within an iterative procedure based on the total energy gradient calculated analytically with respect to the nuclear coordinates. Convergence was determined from the root-mean-square (rms) and the absolute value of the largest component of both gradients and nuclear displacements. The thresholds for the maximum and the rms forces (the maximum and the rms atomic displacements) have been set to 0.00045 and 0.00030 (0.00180 and 0.00120) in atomic units. Geometry optimization was terminated when all four conditions were satisfied simultaneously.[62,63]

III. RESULTS

In this section the perfect rutile structure is presented with the supercell adopted for the doped system (Sec. III A). At fixed geometry, the oxidation state of the iron atom has been studied (Sec. III B) and then the structural relaxation due to the presence of Fe in the lattice has been investigated for the ground state (Sec. III C). The electronic structure is analyzed in terms of the total and projected density of states and Mul-

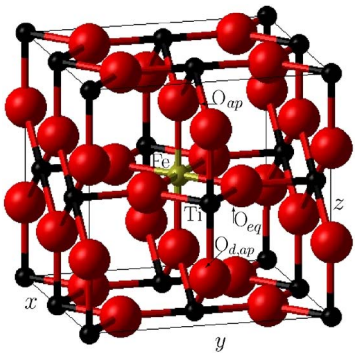

FIG. 1. (Color online) The 24-atom supercell of the iron-doped rutile structure. The small (large) spheres are titanium (oxygen) atoms. The iron ion is located at the center of the cell.

liken partition of the charge and spin density (Sec. III D). In addition, metastable solutions with a localized hole are presented in order to establish the stability of the ground state (Sec. III E). Finally, the magnetic ground state is presented and the exchange coupling constants J evaluated (Sec. III F).

A. Geometry

The rutile structure belongs to the $P4_2/mnm(D_{4h}^{14})$ tetragonal space group and the unit cell, defined by the lattice vectors **a** and **c**, contains two TiO_2 units with Ti ions at (0,0,0) and $(\frac{1}{2},\frac{1}{2},\frac{1}{2})$ and O ions at $\pm(u,u,0)$ and $\pm(u+\frac{1}{2},\frac{1}{2}-u,\frac{1}{2})$.[12,64] The predicted structural parameters, with the percentage deviation from those observed[65] in parenthesis, are (in Å): $\mathbf{a}=4.639(1.14\%)$, $\mathbf{c}=2.981(0.90\%)$, $u=0.306(0.48\%)$, and $\mathbf{V}=64.151(3.23\%)$. This structure is consistent with that predicted in previous calculations.[12]

Each Ti is octahedrally coordinated to six O ions forming a distorted octahedron, with the length of the two apical Ti-O_{ap} bonds slightly longer than the four equatorial Ti-O_{eq} bonds. The calculated (observed) lengths (in Å) are 2.009 (1.976) for Ti-O_{ap} and 1.959 (1.946) for Ti-O_{eq}. The four equatorial oxygen atoms form a rectangle, stretched along **c**, with the titanium atom at the center and with the smaller angle $O_{eq}\hat{T}iO_{eq}$ equal to 80.95° (81.24°).

In order to model iron-doped TiO_2 at a realistic concentration a supercell approach has been adopted. In Fig. 1 an iron-doped 24-atom supercell (S_{24}) is displayed, which is generated by doubling the **c** lattice vector and introducing a $\sqrt{2}\times\sqrt{2}R45°$ expansion of the cell in the **ab** plane. Substitution of Ti with Fe in the cell results in a concentration of $x=0.125$ which is towards the higher end of the range of concentrations that has been realized in practice (see Sec. I).

In Fig. 1 the global Cartesian reference system of the cell used here is also shown. This frame is not conventionally adopted for the description of d orbitals within ligand field theory. In fact the Fe $d_{x^2-y^2}$ and d_{xy} are exchanged and, accordingly, the d_{yz} and d_{xz} orbitals (in the global system) are rotated by 45° with respect to the conventionally local reference system. In the global frame, the e_g states correspond to d_{xy} and $d_{2z^2-x^2-y^2}$ orbitals. The Cartesian frame adopted here is convenient because the density matrix in this orientations of the d orbitals is diagonal.

B. The oxidation state of the iron atom

An essential prerequisite for discussing the magnetic properties of Fe-doped TiO_2 is the identification of the Fe oxidation state, which is potentially coupled very strongly to the nature of the hole states in the host crystal and the local relaxation of the lattice. The formal charge states of TiO_2 within an ionic model are

$$\mathrm{Ti} \rightarrow \mathrm{Ti}^{4+} + 4e^-, \quad 2\mathrm{O} + 4e^- \rightarrow 2\mathrm{O}^{2-}.$$

Upon substitution of the Ti with Fe there are a number of possible formal charge states that might be adopted:

$$\mathrm{Fe} \rightarrow \mathrm{Fe}^{4+} + 4e^-, \quad 2\mathrm{O} + 4e^- \rightarrow 2\mathrm{O}^{2-}, \ 0 \text{ hole}; \tag{1}$$

$$\mathrm{Fe} \rightarrow \mathrm{Fe}^{3+} + 3e^-, \quad 2\mathrm{O} + 3e^- \rightarrow \mathrm{O}^{2-} + \mathrm{O}^-, \ 1 \text{ hole}; \tag{2}$$

$$\mathrm{Fe} \rightarrow \mathrm{Fe}^{2+} + 2e^-, \quad 2\mathrm{O} + 2e^- \rightarrow 2\mathrm{O}^-, \ 2 \text{ holes}; \tag{3}$$

where it is assumed that any holes donated to the lattice are accommodated by the O ions of the lattice as observed in Li-doped MgO (see, for instance, Ref. 66) and in Li-doped NiO.[67,68] The magnetic moment of Fe in the high spin state is $4\mu_B$ for Fe^{4+} and Fe^{2+} (cases 1 and 3) and $5\mu_B$ for Fe^{3+} (case 2). In case 1 this leads to a total spin per cell of $4\mu_B$ but in cases 2 and 3 the total spin also depends on the coupling with unpaired electrons induced in the surrounding lattice.

A number of metastable charge and spin states can be generated in addition to the ground state electronic structure by varying the initial condition of the calculation. In Table I the relative total energy, ionic charges, and spin moments for various states are reported as a function of the total spin per cell S (the difference in number between electrons in a majority and a minority spin state), at the optimized rutile geometry; for completeness solutions that are non-spin-polarized (NSP) and spin polarized but with a total spin of 0 are also reported.

The computed charges reveal a more complex picture than that expected from the simple ionic model and the determination of the Fe oxidation state and of the nature of the unpaired electron(s) associated with the accommodation of hole(s) by the lattice is not straightforward. The nature of the competing states is further analyzed in Table II where the individual d-orbital populations of the Fe ion are presented. For $S=6$, the charge and spin populations of the Fe ion are consistent with an Fe^{3+}-like high spin d^5 state. Interestingly, the two d orbitals pointing towards neighboring O ions which are of e_g type ($d_{2z^2-x^2-y^2}$ and d_{xy} in Table II) have smaller spin and larger charge populations than the t_{2g}-like orbitals indicating a partially covalent nature for the Fe-O interaction which contributes to a decrease of μ_{Fe} ($4.273\mu_B$) from the formal value of $5\mu_B$. In this state there is also a majority (α) spin density delocalized over the six O neighbors. The $S=4$ solution is the ground state and the charge and spin populations of the Fe ion are close to those expected for an Fe^{3+}-like high spin d^5 state, although the spin occupation of the e_g orbital oriented towards the equatorial O ions (d_{xy}) is suppressed ($0.397\mu_B$). In contrast to the $S=6$ solution the unpaired electrons on the neighboring O ions are minority (β) spin. The unpaired electron is delocalized over the O

TABLE I. The energy difference (ΔE, in eV), with respect to the ground state ($S=4$), net atomic charges (q in $|e|$), and spin moments (μ in μ_B) evaluated according to a Mulliken partition of charge and spin densities as a function of the total spin S of the supercell. The adopted geometry is the B3LYP optimized structure of pure rutile TiO_2. NSP denotes the non-spin-polarized solution. In the undoped rutile $q_{Ti}=2.158|e|$ and $q_O=-1.079|e|$.

		q: $Z-(n_\alpha+n_\beta)$				μ: $n_\alpha-n_\beta$			
S	ΔE	Fe	O_{ap}	O_{eq}	Ti	Fe	O_{ap}	O_{eq}	Ti
NSP	1.58	2.042	−1.064	−1.072	2.183				
0	0.86	2.102	−1.074	−1.082	2.184	0.031	0.020	−0.018	0.003
2	0.30	2.106	−1.069	−1.087	2.185	2.104	−0.030	−0.019	0.004
4		2.249	−1.134	−1.088	2.182	3.694	0.121	−0.008	0.028
6	0.65	2.220	−1.088	−1.124	2.188	4.272	0.219	0.255	−0.046

neighbors as in the $S=6$ case but now occupies a crystalline orbital resulting from the hybridization of Fe-d_{xy} and O-$2p$ orbitals.[86]

In the $S=2$ case, the population of the d orbitals is consistent with an Fe^{2+}-like high spin d^6 configuration; this is a complete suppression of the spin in the $d_{x^2-y^2}$ orbital, which is in O_{eq} plane and oriented between a pair of O ions. The two unpaired electrons donated to the lattice have opposite spin to those of the Fe ion. In addition to the reduction of the spin of the d_{xy} orbital observed in the $S=4$ case there is also a similar decrease for the $d_{2z^2-x^2-y^2}$ orbital.

The main finding of this initial survey of the effect of the oxidation state of the Fe ion is that the ground state for Fe-doped rutile TiO_2 corresponds to a high spin state Fe^{3+}-(d^5) configuration with the unpaired electron of the lattice coupled antiparallel to that of the Fe resulting in an overall spin density per cell of $S=4$. The unpaired electron is in a crystalline orbital formed by an hybridization of the Fe-d_{xy} and O-$2p$ atomic orbitals and is thus delocalized among the four nearest neighbor O ions.

C. Structural relaxation

The relaxation of the ions in the surrounding lattice has been performed for the $S=4$ state presented in Sec. III B. In order to illuminate the key interactions, the optimization has been performed in four stages, relaxing (1) the two O_{ap} atoms, (2) the four O_{eq} atoms, (3) all the six nearest neighbors, and (4) all the atomic coordinates inside the supercell. The displacements and gain in energy at each stage are summarized in Table III. It is evident that the four O_{eq} ions experience a breathing-mode relaxation to accommodate the Fe dopant. The displacement of the O_{eq} ions alone accounts for 36% of the total relaxation energy and is the dominant contribution (the displacement of the O_{ap} ions alone accounts for just 5% of the total). The relaxation of O_{ap} ions becomes more significant when performed in conjunction with the O_{eq} ions: ΔE for the optimization of both O_{ap} and O_{ap} yielding about 50% of the total. This cooperative effect is also apparent in the displacements. When optimized separately, O_{eq} and O_{ap} have, respectively, a displacement equal to 68 and 45 % of the full relaxation. In addition to the primary effects of the displacement of O_{eq} and the secondary ones of O_{ap} on the relaxation, it is interesting that the displacement of the $O_{d,ap}$ ions (−0.026 Å), which are the four apical oxygen atoms of the two Ti ions that neighbor Fe (see Fig. 1), relax in a direction opposite to that of the O_{ap} ions. The local distortion of the octahedron containing the Fe ion is documented in Table IV. The decrease of the O_{eq}-O_{eq} distance is accompanied by an increase in O_{ap}-O_{ap}.

In order to check the concentration dependence of these distortions a supercell S_{196} was created by doubling each lattice vectors of S_{24}, resulting in an Fe content of $x=0.0156$ (Table IV). The O-O distances are essentially the same (within 1.5% of that in the S_{24} cell) indicating that the local distortion of the octahedron is close to the dilute limit for $x=\frac{1}{24}$, even though the full relaxation of all the atoms in the supercell entails a further energy gain of 0.3 eV, due to

TABLE II. The charge (q in $|e|$) and spin (μ in μ_B) population of the d atomic orbitals for Fe as a function of S of the entire doped supercell. The d orbital pointing towards oxygen atoms are in bold.

	q: $Z-(n_\alpha+n_\beta)$					μ: $n_\alpha-n_\beta$				
S	$\boldsymbol{d_{2z^2-x^2-y^2}}$	d_{xz}	d_{yz}	$d_{x^2-y^2}$	$\boldsymbol{d_{xy}}$	$\boldsymbol{d_{2z^2-x^2-y^2}}$	d_{xz}	d_{yz}	$d_{x^2-y^2}$	$\boldsymbol{d_{xy}}$
NSP	**0.741**	1.967	0.618	1.847	**0.675**					
0	**0.836**	1.186	1.178	1.836	**0.746**	**−0.018**	−0.791	0.801	0.035	**0.004**
2	**0.834**	1.134	1.124	1.936	**0.751**	**0.182**	0.847	0.859	0.023	**0.183**
4	**1.271**	1.120	1.140	1.084	**1.007**	**0.722**	0.864	0.847	0.896	**0.348**
6	**1.200**	1.085	1.084	1.053	**1.246**	**0.787**	0.896	0.900	0.920	**0.753**

TABLE III. The distance (Å) between Fe and its neighbors is given in the first row of data. In the second column, the set of atoms whose coordinates have been optimized is given for both S_{24} and S_{196} supercells. ΔE (in meV) is the relaxation energy evaluated with respect to the structure without geometry optimization (first row of data). The displacements (Å) are given in italics; a negative value means a relaxation towards the iron atom and blanks indicate no displacement. The underlined values indicated cases in which the relaxation alters the distance ordering of the neighbors.

	ATOM	ΔE	$4O_{eq}$	$2O_{ap}$	2Ti	$4O_{d,eq}$	$4O_{d,ap}$	4Ti	4Ti	8O	$2O_{ap}$	8O	4Ti	$4O_{eq}$
			1.959	2.009	2.981	3.518	3.594	3.603	3.603	4.125	4.552	4.611	4.639	4.649
S_{24}	$2O_{ap}$	−7.5	1.914	2.026	2.981	3.518	3.594	3.603	3.603	4.125	4.535	4.611	4.639	4.649
				+0.017							*−0.017*			
	$4O_{eq}$	−59.3	1.920	2.009	2.981	3.518	3.594	3.603	3.603	4.125	4.552	4.611	4.639	4.675
			−0.040											*+0.040*
	$6O_{ap,eq}$	−81.0	1.914	2.038	2.981	3.518	3.594	3.603	3.603	4.125	4.523	4.611	4.639	4.680
			−0.046	*+0.029*							*−0.029*			*+0.046*
	All	−167.0	1.902	2.047	2.981	3.517	3.580	3.593	3.597	4.131	4.514	4.606	4.639	4.693
			−0.059	*+0.038*		*−0.004*	*−0.026*	*−0.026*	*−0.016*	*+0.010*	*−0.038*	*−0.018*		*−0.059*
S_{196}	All	−314.8	1.883	2.080	2.913	3.523	3.582	3.593	3.656	4.135	4.578	4.589	4.655	4.637
			−0.078	*+0.072*	*−0.067*	*+0.005*	*−0.012*	*−0.017*	*+0.065*	*+0.010*	*+0.026*	*+0.023*	*+0.015*	*−0.011*

both a larger displacement of the neighboring oxygen atoms of Fe and a further relaxation of the atoms not included in S_{24}. Accordingly, in what follows the S_{24} cell is taken to be adequate as a representation of the dilute limit.

D. Electronic structure

The projected total density of states (DOS) of undoped rutile TiO_2 is displayed in Fig. 2(a). The upper valence band (−10.6−−4.5 eV) has predominantly O-2*p* character with some hybridization with Ti-3*d* orbitals, while the lower conduction band has Ti-3*d* character. The computed width of the upper valence band is 6.13 eV, in agreement with that observed [5–6 eV[69,70]] and the computed band gap is 3.40 eV in reasonable agreement with that observed in optical spectroscopy of ~3 eV.[69,71–73] This reliable reproduction of the observed electronic structure is an important feature of the hybrid exchange approximation.

The spin-polarized DOS of the doped system is presented in Fig. 2(b). The Fe ion contributes a narrow, spatially localized, band of majority spin states below the bottom of the upper valence band and a broad spectrum of more delocalized states which are hybridized with the O-2*p* band. These features are consistent with the discussion of the Fe oxidation state above. These main features of the DOS are similar to those computed for ilmenite ($FeTiO_3$)[47] indicating that these essential features of the electronic structure of the Fe^{3+} ion in a titanate host lattice are fairly independent of concentration, which is consistent with a highly localized picture of the electronic structure of the Fe^{3+} ion. There is also evidence for some hybridization between the Fe-3*d* and O-2*p* orbitals. In particular, the Fe-derived minority spin states can be attributed mainly to the *d* orbitals oriented towards O_{eq} and are due to the interaction with the unpaired minority-spin state electron delocalized over the four O_{eq} ions.

TABLE IV. Geometrical parameters of the octahedron in terms of the distance (Å) between O_{eq} and O_{eq} neighboring the iron impurity for the geometry optimization performed.

Supercell		Relaxed atoms	Distance		
			O_{eq}-O_{eq}	O_{eq}-O_{ap}	O_{ap}-O_{ap}
			2.54/2.98	2.81	4.02
S_{24}	1×1×1	O_{ap}		2.82	4.05
		O_{eq}	2.50/2.91	2.78	4.02
		O_{ap} and O_{eq}	2.50/2.90	2.79	4.08
		All	2.49/2.87	2.79	4.10
S_{196}	2×2×2	All	2.47/2.84	2.81	4.16

Upon doping, a number of defect states are generated in the band gap. About 2 eV above the valence band maximum (VBM) there is a majority spin state (mainly due to the Fe-*d* orbital pointing towards O_{eq} and to the O_{eq}-p_x and O_{eq}-p_y ones). In the minority spin states a feature exists 2.38 eV above the VBM (which is 0.05 eV lower than the VBM in the majority spin states) these are the crystal field split Fe-*d* states. The presence of these minority spin states in the band gap has been suggested previously on the basis of molecular orbital diagrams for the isolated $(Fe^{3+}O_6)^{9-}$ cluster.[74]

The localized majority-spin states, which are in the energy range from −12.5 to −10.5 eV, can be analyzed further in terms of the contributions of the individual *d* orbitals and a simply ionic picture of the interactions (Fig. 3). In the distorted octahedron the degeneracy of the *d* orbitals is lifted but they can be grouped into t_{2g}-like and e_g-like subbands. Of the e_g levels that are oriented towards the O_{ap} the d_{z^2} is lower in energy than the d_{xy}, which interacts with the O_{eq}, as the Fe-O_{ap} distance is slightly longer than the Fe-O_{eq} distance (1.902 vs 2.047 Å). Within the t_{2g} derived states, the $d_{x^2-y^2}$ orbital, which is in the O_{eq} plane, is the most stable and is sensitive to the position of the neighboring O_{eq} atoms.

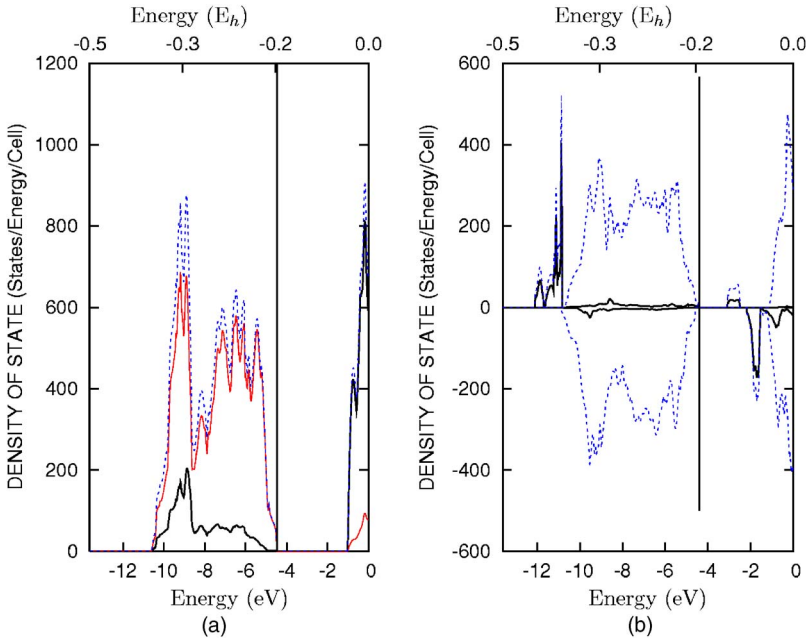

FIG. 2. (Color online) The total DOS (dashed-line) of the 24-atom supercell (a) and after iron-doping and geometry optimization (b). The DOS are projected in (a) on the oxygen (thin continuous line) and titanium (thick continuous line) atoms and in (b) on the iron (thick continuous line) atom. The top of valence bands is indicated by the vertical line. In (b) positive (negative) density values refer to majority (minority) spin states.

Upon relaxation of the oxygen neighbors, and in particular of O_{eq}, the angle $O_{eq}FeO_{eq}$ bisected by the x axis increases from 80.95° to 81.89°, the consequent decrease of electronic repulsion stabilizes this energy level as is apparent when comparing Figs. 3(a)–3(c). The width of the $d_{x^2-y^2}$ derived states can be explained considering that along the x axis the pillar of octahedra shares an edge. The stabilization effect due to the edge sharing of the octahedra is partially evident for d_{xz} and can also rationalize the lower energy of d_{xz} with respect to d_{yz} (even though d_{xz} bisects the smaller O_{eq}-Fe-O_{eq} angle). Then the d_{yz} peak is narrower since it is not perturbed by the presence of edge-sharing octahedron.

The Fe-O interaction can also be analyzed using the charge and spin density maps displayed in Fig. 4. The plots are drawn in two different planes in order to expose the differences between the Fe-O_{eq} and Fe-O_{ap} interactions: the former defined by the Fe ion and two of the O_{eq}, the latter defined by Fe, O_{eq}, and O_{ap}. Along the Fe-O_{ap} direction the charge density map reveals a rather ionic picture of the bonding with near spherical charge density around the O and Fe ions. In the Fe-O_{eq} direction the charge density is more concentrated in the bond and spin density is consistent with the strong Fe(α-d_{xy})-O(β-2p) interaction, suggested by the DOS. On the O_{eq} centers the hexapole consists of minority spin p orbitals oriented towards the Fe atom and majority spin p orbitals orthogonal to these and, as a consequence, the overall spin on O_{eq} is small (see Tables I and IV and Fig. 4).

As the role of electronic exchange is expected to be crucial in this system the sensitivity of the local electronic structure to the percentage of the Fock exchange used in the hybrid functional has been investigated. The variation in the Mulliken spin and charge populations of the Fe-d orbitals are plotted in Fig. 5. A substantial difference in the behavior of the e_g and t_{2g} orbitals is evident. The former states are characterized by a lower spin density, mainly due to hybridization with the neighboring oxygen atoms, this is especially evident for the d_{xy} orbital interacting with O_{eq}. The effect of the treatment of electronic exchange and correlation on the

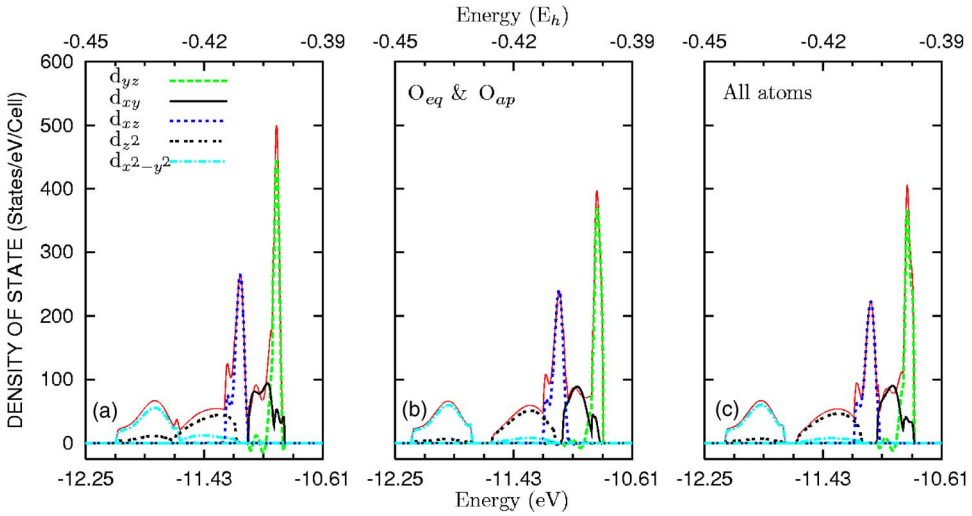

FIG. 3. (Color online) The projected DOS on the atomic d orbitals of the iron impurity. Three cases have been shown: (a) no geometry relaxation is performed after the creation of the defect, (b) only the coordinate of the oxygen atoms nearest neighbors of the iron have been optimized, (c) all the 24 atoms in the supercell are allowed to relax. Black lines refer to d orbitals pointing towards the oxygen nearest neighboring atoms: continuous line for O_{eq} and dashed one for O_{ap}. The thin line (gray/red) is the projection on the iron atomic orbitals.

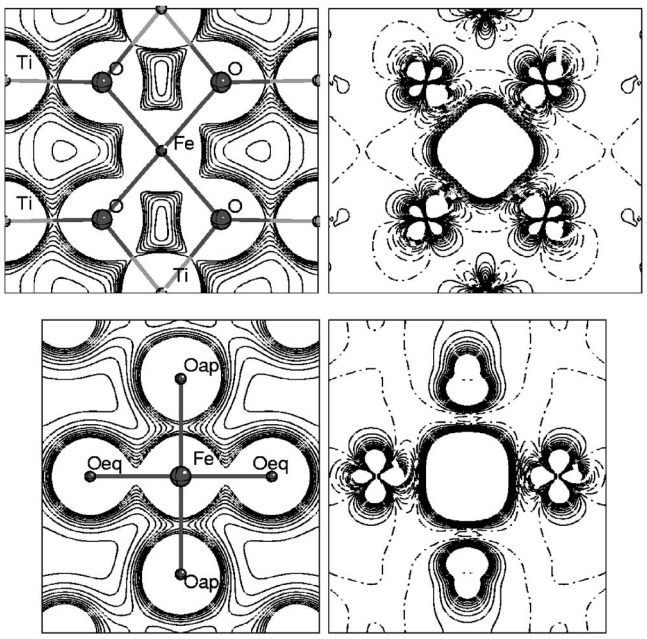

FIG. 4. Total (left) and spin (right) density maps in two planes; the first (upper panel) defined by the Fe and $2O_{eq}$ atoms (top) and the second (lower panel) with Fe, O_{ap}, and O_{eq} (bottom). Ten total density contour lines are drawn from 0.01 to $+0.10|e|/\text{Bohr}^3$. Spin isodensity lines range from −0.001 (negative dashed lines) to $+0.001|e|/\text{Bohr}^3$ (positive continuous lines) by increment of $0.0001|e|/\text{Bohr}^3$.

d_{xy} spin population is most striking. As the Fock exchange component is increased the spin density increases rapidly due to the increasing localization of the crystalline orbital and the decreasing interaction with the delocalized O-2p hole. The plateau in the total population of the d_{xy} orbital above 40% is particularly significant in the light of the evidence that more than about 25% Fock exchange is typically needed to describe the overall electronic structure of crystalline insulators.[75–78] It is important to note that the effect of Fock exchange is documented here in order to establish the sensitivity of the solution to the treatment of electronic exchange and not to suggest that the functional should be varied; the B3LYP functional is a well-documented and widely used approximation.

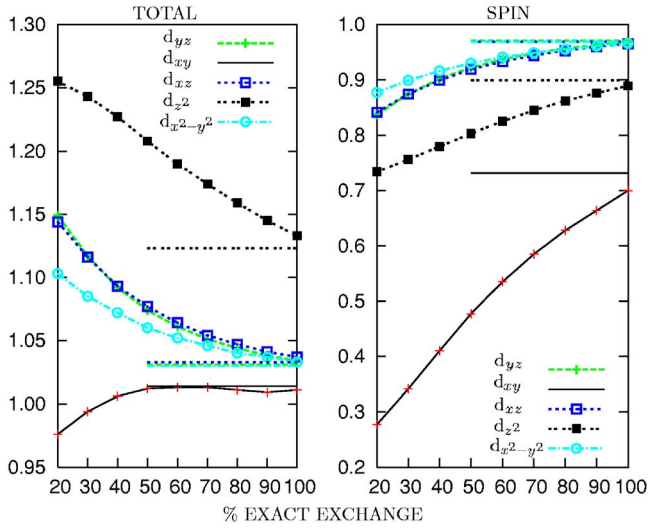

FIG. 5. (Color online) The Mulliken total and spin populations of the single Fe-d orbitals as function of the percentage of the exact exchange. The value 20% corresponds to B3LYP.

E. The possibility of self-trapping of the hole state

The strong interplay between the geometry and the electronic structure can be exploited to generate metastable states in which self-trapping of the hole occurs at O_{ap} and O_{eq} in various p states and with spin either parallel or antiparallel to the spin of the Fe ion. There is then the possibility that the resultant lattice distortion lowers the energy of the self-trapped state significantly. Accordingly, a study of the local environment of the iron near an oxygen ion with a trapped hole has been performed. As the Hartree-Fock approximation displays a well-documented tendency to over localized states in magnetic insulators this approach is used to generate initial guesses for the localized states and to document the strongly interacting limit.

It is evident from HF data in Table V that the lowest energies solutions have the p orbital with the unpaired electron orthogonal to the plane identified by unit $FeOTi_2$; the localization at O_{eq} (with a p_z character) being about 0.2 eV more favorable than at O_{ap} (p_y). In both cases the spin of the unpaired electron is aligned with Fe and when flipping its spin state there is an energy increase of $\sim 0.02-0.04$ eV.

TABLE V. The energy (eV) within the Hartree-Fock level of theory as function of the localization of the unpaired electron at the oxygen position (O_{ap} and O_{eq}) in each p orbital for both the spin states. The first two rows are reported with respect to the minimum value, labeled by zero. The nonrelaxed and FeO_6-relaxed lines refer, respectively, to iron-doped TiO_2 at the experimental geometry and to the same structure after a geometry optimization of the octahedron FeO_6; the energy difference between the two cases is given in the relaxation line. The blank means that the value has not been calculated.

	$O_{ap}(p_x)$		$O_{ap}(p_y)$		$O_{ap}(p_z)$		$O_{eq}(p_x/p_y)$		$O_{eq}(p_z)$	
	α	β	α	β	α	β	α	β	α	β
Nonrelaxed	2.26	2.31	0.83	0.86	2.67	2.07	2.06	1.59	0.65	0.67
FeO_6-relaxed	1.32	1.38	0.08	0.13	1.60	1.36			zero	0.04
Relaxation	0.95	0.94	0.75	0.74	1.06	0.72			0.65	0.63

TABLE VI. The energy (eV), Fe displacement Δr_{Fe} (Å), and distance (Å) between Fe and its neighbors and Mulliken spin moment ν as a function of the delocalization/localization of the unpaired electron at oxygen position(s), indicated in the first column. NL means that the unpaired electron is shared among neighboring oxygen atoms of Fe; α-$\mathrm{O}_{\mathrm{eq}}(p_z)$ corresponds to the solution with the unpaired electron localized in a p_z orbital of O_{eq} in a majority spin state (α). The data refer to a fully optimization of the internal atomic coordinates. Underlined values indicate the oxygen ions where the unpaired electron is localized.

	S	ΔE	Δr_{Fe}	$d_{\mathrm{Fe\text{-}O_{eq}}}$				$d_{\mathrm{Fe\text{-}O_{ap}}}$		μ_{Fe}	$\mu_{\mathrm{O_{eq}}}$				$\mu_{\mathrm{O_{ap}}}$	
NL	4	zero		1.902				2.047		3.582	0.032				0.091	
α-$\mathrm{O}_{\mathrm{eq}}(p_z)$	6	0.17	0.079	1.959	1.974	2.003	2.069	2.015		4.283	0.101	0.122	0.108	0.948	0.104	
β-$\mathrm{O}_{\mathrm{eq}}(p_z)$	4	0.21	0.058	1.963	1.976	1.999	2.050	2.019		4.285	0.103	0.125	0.108	−0.800	0.075	
α-$\mathrm{O}_{\mathrm{ap}}(p_y)$	6	0.45	0.109	2.008				1.990	2.045	4.271	0.155				0.073	0.857
β-$\mathrm{O}_{\mathrm{ap}}(p_y)$	4	0.55	0.127	2.011				1.978	2.058	4.279	0.107				0.054	−0.806
NL	6	0.64		2.027				2.025		4.289	0.226				0.102	

This finding is also confirmed when the octahedron FeO_6 distortion is taken into account. Within the HF approximation the α-$\mathrm{O}_{\mathrm{eq}}(p_z)$ solution is ~2 eV lower in energy than the state in which there is delocalization of the unpaired electron among oxygen atoms nearest neighboring of Fe.

The displacements computed within HF of the atoms in the FeO_6 octahedron for the four lowest energy cases in Table V have been exploited to define initial geometries for hybrid exchange calculations in order to generate potential self-trapped hole states. From the data in Table VI it is evident that the localization of an unpaired electron in the α-$\mathrm{O}_{\mathrm{eq}}(p_z)$ state (where $\mu_{\mathrm{O_{eq}}}=0.948 \sim \mu_{p_z}=0.842$) is more favorable than all other solutions with a localized unpaired electron. Furthermore the stability order $[\alpha\text{-}\mathrm{O}_{\mathrm{eq}}(p_z) < \beta\text{-}\mathrm{O}_{\mathrm{eq}}(p_z) < \alpha\text{-}\mathrm{O}_{\mathrm{ap}}(p_y) < \beta\text{-}\mathrm{O}_{\mathrm{ap}}(p_y)]$ of the HF approximation is preserved. However, the results presented in Table VI establish clearly that the delocalized $S=4$ state (investigated in Secs. III C and III D) is lower in energy even after local distortions associated with the self-trapping of the hole.

F. The magnetic coupling

In the previous sections the nature of the spin density associated with each Fe dopant has been established and seen to be essentially localized on Fe-d^5 and nearest neighboring oxygen atoms. It is the purpose of this section to examine the magnetic interactions between these localized spins that determine the macroscopic magnetic properties. At fixed dopant concentration the energy of parallel and antiparallel configurations of the spins is computed in suitable supercells of the fundamental cell. Cells containing 48 atoms created by doubling along either the **a**, **b**, or **c** directions are used to study nearest neighbor interactions and cells of 96 atoms doubled in two directions used to generate states in which there is antiparallel alignment along two directions.

The energies of these various states are presented in Table VII; as expected, the energy scale of magnetic ordering is a few meV per Fe much smaller than the charge ordering energy scale of about one half eV (see Table I), as observed previously in ilmenite.[47] This disparity in energy scales supports the assumption that studying the structural degrees of freedom in the ferromagnetic configuration is sufficient (Sec. III C). Indeed, if further structural relaxation is performed in the presence of an antiferromagnetic alignment the energy gain is negligible (~0.02 meV). For coupling along all directions considered here, the antiparallel alignment of spins is more stable than parallel (see Table VII) and the most stable state is antiferromagnetic with antiparallel coupling in all directions. The coupling is about 2–3 times stronger along **c** than along **b** and **a**. Within a simple Ising model, the computed exchange coupling constants among impurities are $J_{\mathbf{a}}=3.2$ K, $J_{\mathbf{b}}=4.8$ K, and $J_{\mathbf{c}}=11.0$ K, where the spin has been taken to be $|S_{\mathrm{Fe}}=\frac{5}{2}|$, which is the formal value of Fe^{3+} in a high spin state. The calculations on the quadruple cell establish that the magnetic coupling is essentially nearest neighbor and additive, as there is a deviation of less than 2% between the stabilization energy ΔE given in Table VII and that computed from the nearest neighbor interactions along the crystallographic directions $J_{\mathbf{a}}$, $J_{\mathbf{b}}$, and $J_{\mathbf{c}}$.

The prediction here, that the coupling favors antiparallel spins in all directions within the lattice, is not consistent with previous work which reported a ferromagnetic coupling for certain directions.[45] However, the previous study was conducted at a much higher concentration ($x=0.5$) than the present study. At $x=0.5$ it is likely that the spin density induced by the dopants overlaps as is also evidenced by the very different Fe magnetic moment reported previously.[45,46]

TABLE VII. The energy difference (ΔE) per $FeTi_7O_{16}$ formula unit E with respect to the ferromagnetic state as a function of the supercell size and shape. i corresponds to the direction(s) along which the impurities are coupled antiferromagnetically. The magnetic moments of Fe (μ_{Fe}) for each case are very close to the ferromagnetic value $3.58\mu_B$.

	Supercell				
i	Size	Shape	ΔE(meV)	$\mu_{\mathrm{Fe}}(\mu_B)$	
a	48	**2a**×**1b**×**1c**	−3.5	3.58	−3.57
b	48	**1a**×**2b**×**1c**	−5.1	3.59	−3.57
c	48	**1a**×**1b**×**2c**	−11.9	3.58	−3.57
a,**b**	96	**2a**×**2b**×**1c**	−8.7	3.59	−3.57
a,**c**	96	**2a**×**1b**×**2c**	−15.2	3.58	−3.57
b,**c**	96	**1a**×**2b**×**2c**	−17.0	3.58	−3.57
a,**b**,**c**	48		−20.2	3.58	−3.57

The value of μ_{Fe} varied in the range $1.68-2.67\mu_B$ and was found to be very sensitive to the distribution of iron in the supercells. In constant, as can be seen from Table VII, the present value of μ_{Fe} ($\sim\pm3.58\mu_B$) is independent of the magnetic order. This discrepancy is also exacerbated by the use of the local spin density approximation in previous studies which has a well-documented tendency to over-delocalization of the states in transition metal oxides.

As the hybrid functional used here correctly describes the balance between localized and delocalized states, it can be concluded that the calculations reported here establish that well separated Fe dopants at $x=0.125$ yield large local magnetic moments which do not order to form a ferromagnetic state that would be stable at room temperature.

IV. CONCLUSIONS

The magnetic ground state of Fe-doped rutile TiO_2, an oxide-based diluted magnetic semiconductor, has been investigated using hybrid-exchange density-functional theory. A 24-atom supercell of rutile with an Fe atom substituted for Ti has been used to simulate the dilute content of dopant ($Fe_xTi_{1-x}O_2$, $x=0.125$). The fact that this supercell represents the dilute limit is established by direct comparisons of the relaxation energy and geometrical distortions of a 192-supercell ($x=0.0156$).

A detailed study of the oxidation state of Fe and the related presence and nature of the holes donated to the lattice has established that the ground state corresponds to a high spin state consistent with an Fe^{3+}-(d^5) configuration with the unpaired electron of the lattice coupled antiparallel to that of the Fe resulting in an overall spin density per cell of $S=4$. The analysis of the electronic structure in terms of Mulliken charges, total and spin density maps, and total and projected density of states has identified the hole state as a delocalized orbital formed by the hybridization of the Fe-d orbital pointing towards the four O_{eq} and O_{eq}-$2p$ orbitals.

The stability of this state with respect to self-trapping of the hole has been found to be sensitive to the treatment of the electronic exchange and correlation: within the HF level of theory the lowest-energy solution corresponds to an unpaired electron trapped at an oxygen position nearest neighboring of Fe, while within the hybrid exchange approximation all self-trapped states are metastable with respect to the delocalized solution.

The calculation of the ferromagnetic and antiferromagnetic coupling of the spin associated with impurities establishes that, for the well separated Fe dopants at $x=0.125$, the large local magnetic moments are insensitive to the magnetic order and do not couple to form a ferromagnetic state that would be stable at room temperature, in agreement with previous experimental works.[32,37,40]

From the apparent independence of the magnetic moment and coupling mechanism on the Fe content it seems likely that this conclusion can be extended to smaller concentrations. The reported observations of ferromagnetism have yielded a wide range of magnetic moments per Fe dopant which appear to be sensitive to the growth conditions and in particular the oxygen partial pressure.[31,79,80] In view of this it seems possible that the ferromagnetism is due to a mechanism which is based on variations in the oxygen stoichiometry in addition to the substitutional incorporation of Fe in the host crystal.[81–84].

ACKNOWLEDGMENTS

G.M. thanks EPSRC for Grant No. GR/S13422/01 and L. Pisani for useful discussions.

*Electronic address: g.mallia@imperial.ac.uk

[1] U. Diebold, Surf. Sci. Rep. **48**, 53 (2003).
[2] B. Silvi, N. Fourati, R. Nada, and C. R. A. Catlow, J. Phys. Chem. Solids **52**, 1005 (1991).
[3] P. Reinhardt and B. A. Hess, Phys. Rev. B **50**, 12015 (1994).
[4] K. M. Glassford and J. R. Chelikowsky, Phys. Rev. B **46**, 1284 (1992).
[5] C. Lee, P. Ghosez, and X. Gonze, Phys. Rev. B **50**, 13379 (1994).
[6] M. Ramamoorthy, D. Vanderbilt, and R. D. King-Smith, Phys. Rev. B **49**, 16721 (1994).
[7] P. J. D. Lindan, N. M. Harrison, J. M. Holender, M. J. Gillan, and M. C. Payne, Surf. Sci. **364**, 431 (1996).
[8] P. Reinhardt, B. A. Heß, and M. Causa', Int. J. Quantum Chem. **58**, 297 (1996).
[9] P. J. D. Lindan, J. Muscat, S. Bates, N. M. Harrison, and M. Gillan, Faraday Discuss. **106**, 135 (1997).
[10] K. Rosciszewski, K. Doll, B. Paulus, P. Fulde, and H. Stoll, Phys. Rev. B **57**, 14667 (1998).
[11] L. S. Dubrovinsky, N. A. Dubrovinskaia, V. Swamy, J. Muscat, N. M. Harrison, R. Ahuja, B. Holm, and B. Johansson, Nature (London) **410**, 653 (2001).
[12] J. Muscat, V. Swamy, and N. M. Harrison, Phys. Rev. B **65**, 224112 (2002).
[13] Y. Matsumoto, M. Murakami, T. Shono, T. Hasegawa, T. Fukumura, M. Kawasaki, P. Ahmet, T. Chikyow, S. Koshihara, and H. Koinuma, Science **291**, 854 (2001).
[14] Y. Matsumoto, R. Takahashi, M. Murakami, T. Koida, X.-J. Fan, T. Hasegawa, T. Fukumura, M. Kawasaki, S. Koshihara, and H. Koinuma, Jpn. J. Appl. Phys., Part 2 **40**, L1204 (2001).
[15] W. K. Park, R. J. Ortega-Hertogs, J. S. Moodera, A. Punnoose, and M. S. Seehra, J. Appl. Phys. **91**, 8093 (2002).
[16] W. Wang, J. Dai, J. Tang, D.-T. Jiang, Y. Chen, J. Fang, J. He, W. Zhou, and L. Spinu, J. Supercond. **16**, 155 (2002).
[17] Z. Wang, J. Tang, L. D. Tung, W. Zhou, and L. Spinu, J. Appl. Phys. **93**, 7870 (2003).
[18] Z. Wang, W. Wang, J. Tang, L. D. Tung, L. Spinu, and W. Zhou, Appl. Phys. Lett. **83**, 518 (2003).
[19] T. Fukumura *et al.*, Jpn. J. Appl. Phys., Part 2 **42**, L105 (2003).
[20] T. Fukumura, Y. Yamada, H. Toyosaki, T. Hasegawa, H. Koinuma, and M. Kawasaki, Appl. Surf. Sci. **223**, 62 (2004).
[21] T. Ohsawa, Y. Matsumoto, and H. Koinuma, Appl. Surf. Sci. **223**, 84 (2004).

[22] N. H. Hong, W. Prellier, J. Sakai, and A. Hassini, Appl. Phys. Lett. **84**, 2850 (2004).
[23] N. H. Hong, J. Sakai, W. Prellier, A. Hassini, A. Ruyter, and F. Gervais, Phys. Rev. B **70**, 195204 (2004).
[24] N. H. Hong, J. Sakai, and W. Prellier, J. Magn. Magn. Mater. **281**, 347 (2004).
[25] E. C. Kim, S. H. Moon, S. I. Woo, J. H. Cho, Y. G. Joh, and D. H. Kim, Solid State Commun. **132**, 477 (2004).
[26] Z. Wang, J. Tang, Y. Chen, L. Spinu, W. Zhou, and L. D. Tung, J. Appl. Phys. **95**, 7384 (2004).
[27] Z. Wang, J. Tang, H. Zhang, V. Golub, L. Spinu, and L. D. Tung, J. Appl. Phys. **95**, 7381 (2004).
[28] N. H. Hong, J. Sakai, W. Prellier, and A. Ruyter, J. Phys. D **38**, 816 (2005).
[29] T. Fukumura, H. Toyosaki, and Y. Yamada, Semicond. Sci. Technol. **20**, S103 (2005).
[30] R. Janisch, P. Gopal, and N. A. Spaldin, J. Phys.: Condens. Matter **17**, R657 (2005).
[31] R. Suryanarayanan, V. M. Naik, P. Kharel, P. Talagala, and R. Naik, J. Phys.: Condens. Matter **17**, 755 (2005).
[32] K. Inaba, T. Hitosugi, Y. Hirose, Y. Furubayashi, G. Kinoda, Y. Yamamoto, T. Kim, H. Fujioka, T. Shimada, and T. Hasegawa, Jpn. J. Appl. Phys., Part 2 **45**, L114 (2006).
[33] A. R. Bally, P. E. S. E. N. Korobeinikova, F. Lévy, and F. Bussy, J. Phys. D **31**, 1149 (1998).
[34] S. Wolf, D. Awschalom, R. Buhrman, J. Daughton, S. von Molnár, M. L. Roukes, A. Y. Chtchelkanova, and D. M. Treger, Science **294**, 1488 (2001).
[35] Y. L. Soo, G. Kioseoglou, S. Kim, Y. H. Kao, P. S. Devi, J. Parise, R. J. Gambino, and P. I. Gouma, Appl. Phys. Lett. **81**, 655 (2002).
[36] M. L. Cui, J. Zhu, X. Y. Zhong, Y. G. Zhao, and X. F. Duan, Appl. Phys. Lett. **85**, 1698 (2004).
[37] X. H. Wang, J.-G. Li, H. Kamiyama, M. Katada, N. Ohashi, Y. Moriyoshi, and T. Ishigaki, J. Am. Chem. Soc. **127**, 10982 (2005).
[38] L. Sangaletti, M. C. Mozzati, P. Galinetto, C. B. Azzoni, A. Speghini, M. Bettinelli, and G. Calestani, J. Phys.: Condens. Matter **18**, 7643 (2006).
[39] T. R. Sandin, D. Schroeer, and C. D. Spencer, Phys. Rev. B **13**, 4784 (1976).
[40] L. Balcells, C. Frontera, F. Sandiumenge, A. Roig, B. Martínez, J. Kouam, and C. Monty, Appl. Phys. Lett. **89**, 122501 (2006).
[41] D. L. Carter and A. Okaya, Phys. Rev. **118**, 1485 (1960).
[42] G. J. Lichtenberger and J. R. Addison, Phys. Rev. **184**, 381 (1969).
[43] Y. J. Kim, S. Thevuthasan, T. Droubay, A. S. Lea, C. M. Wang, V. Shutthanandan, S. A. Chambers, R. P. Sears, B. Taylor, and B. Sinkovic, Appl. Phys. Lett. **84**, 3531 (2004).
[44] L. Errico, M. Weissmann, and M. Renteria, Physica B **354**, 338 (2004).
[45] L. A. Errico, M. Renteria, and M. Weissmann, Phys. Rev. B **72**, 184425 (2005).
[46] L. Errico, M. Weissmann, and M. Renteria, Phys. Status Solidi B **241**, 2399 (2004).
[47] N. C. Wilson, J. Muscat, D. Mkhonto, P. E. Ngoepe, and N. M. Harrison, Phys. Rev. B **71**, 075202 (2005).
[48] N. C. Wilson, S. P. Russo, J. Muscat, and N. M. Harrison, Phys. Rev. B **72**, 024110 (2005).
[49] A. W. J. Muscat and N. M. Harrison, Chem. Phys. Lett. **342**, 397 (2001).
[50] X.-B. Feng and N. M. Harrison, Phys. Rev. B **69**, 035114 (2004).
[51] M. Schmidt, W. R. II, P. G. Radaelli, K. Refson, N. M. Harrison, and S. W. Cheong, Phys. Rev. Lett. **92**, 056402 (2004).
[52] C. Franchini, V. Bayer, R. Podloucky, J. Paier, and G. Kresse, Phys. Rev. B **72**, 045132 (2005).
[53] J. E. Peralta, J. Heyd, G. E. Scuseria, and R. L. Martin, Phys. Rev. B **74**, 073101 (2006).
[54] D. Kasinathan *et al.*, Phys. Rev. B **74**, 195110 (2006).
[55] P. J. Hay, R. L. Martin, J. Uddin, and G. E. Scuseria, J. Chem. Phys. **125**, 034712 (2006).
[56] V. R. Saunders, R. Dovesi, C. Roetti, R. Orlando, C. M. Zicovich-Wilson, N. M. Harrison, K. Doll, B. Civalleri, I. J. Bush, P. D'Arco, and M. Llunell, CRYSTAL03 User's Manual, Università di Torino, Torino, 2003.
[57] J. Muscat, Ph.D. thesis, University of Manchester, Manchester, 1999.
[58] J. Muscat, N. M. Harrison, and G. Thornton, Phys. Rev. B **59**, 2320 (1999).
[59] www.crystal.unito.it/basis-sets/ptable.html
[60] A. D. Becke, J. Chem. Phys. **98**, 5648 (1993).
[61] C. Pisani, R. Dovesi, and C. Roetti, *Hartree-Fock ab initio Treatment of Crystalline Systems*, Vol. 48 of Lecture Notes in Chemistry (Springer Verlag, Heidelberg, 1988).
[62] K. Doll, V. Saunders, and N. M. Harrison, Int. J. Quantum Chem. **82**, 1 (2001).
[63] B. Civalleri, P. D'Arco, R. Orlando, V. Saunders, and R. Dovesi, Chem. Phys. Lett. **348**, 131 (2001).
[64] G. Cangiani, A. Baldereschi, M. Posternak, and H. Krakauer, Phys. Rev. B **69**, 121101(R) (2004).
[65] J. K. Burdett, T. Hughbanks, G. J. Miller, J. W. Richardson, and J. V. Smith, J. Am. Chem. Soc. **109**, 3639 (1987).
[66] A. Lichanot, C. Larrieu, R. Orlando, and R. Dovesi, J. Phys. Chem. Solids **59**, 7 (1998).
[67] P. Kuiper, G. Kruizinga, J. Ghijsen, G. A. Sawatzky, and H. Verweij, Phys. Rev. Lett. **62**, 221 (1989).
[68] W. C. Mackrodt, N. M. Harrison, V. R. Saunders, N. L. Allan, and M. D. Towler, Chem. Phys. Lett. **250**, 66 (1996).
[69] D. W. Fisher, Phys. Rev. B **5**, 4219 (1972).
[70] Z. Zhang, S. P. Jeng, and V. E. Henrich, Phys. Rev. B **43**, 12004 (1991).
[71] H. Tang, K. Prasad, R. Sanjinès, P. E. Schmid, and F. Lévy, J. Appl. Phys. **75**, 2042 (1994).
[72] A. Ferreira da Silva, I. Pepe, C. Persson, J. Souza de Almeida, C. Moyses Araujo, R. Ahuja, B. Johansson, C. Y. An, and J.-H. Guo, Phys. Scr. **T109**, 180 (2004).
[73] K. F. Hellwege and O. Madelung, *Numerical Data and Functional Relationships in Science and Technology*, Vol. 17(g) of New Series, Group III (Landolt-Bornestein, Berlin, 1984).
[74] D. M. Sherman, Phys. Chem. Miner. **14**, 355 (1987).
[75] R. L. Martin and F. Illas, Phys. Rev. Lett. **79**, 1539 (1997).
[76] F. Illas and R. L. Martin, J. Chem. Phys. **108**, 2519 (1998).
[77] I. P. R. Moreira, F. Illas, and R. L. Martin, Phys. Rev. B **65**, 155102 (2002).
[78] F. Corà, M. Alfredsson, G. Mallia, D. Middlemiss, W. Mackrodt, R. Dovesi, and R. Orlando, *Principles and Applications of Density Functional Theory in Inorganic Chemistry II*, Vol. 113 of Structure and Bonding, edited by N. Kaltsoyannis and J. E. McGrady (Springer-Verlag, Heidelberg, 2004).
[79] W. Prellier, A. Fouchet, and B. Mercey, J. Phys.: Condens. Matter

15, R1583 (2003).
[80] T. C. Kaspar *et al.*, Phys. Rev. Lett. **95**, 217203 (2005).
[81] M. Venkatesan, C. B. Fitzgerald, and J. M. D. Coey, Nature (London) **430**, 630 (2004).
[82] J. M. D. Coey, M. Venkatesan, and C. B. Fitzgerald, Nat. Mater. **4**, 173 (2005).
[83] M. S. Park, S. K. Kwon, and B. I. Min, Phys. Rev. B **65**, 161201(R) (2002).
[84] H. Weng, X. Yang, J. Dong, H. Mizuseki, M. Kawasaki, and Y. Kawazoe, Phys. Rev. B **69**, 125219 (2004).
[85] $1E_h = 27.2114$ eV $= 4.35974 \times 10^{-18}$ J.
[86] The overall spin on O_{eq} is small (Table I) but as is evident from the analysis of the spin density (Sec. III D, Fig. 1) that the total spin is a combination of two significant components; the minority spin state of the unpaired electron delocalized within the four $O_{eq\text{-}p}$ orbitals oriented towards the Fe atom and two perpendicular *p*-like orbitals with opposite spin polarization.